Journal of Materials Chemistry C

PAPER

View Article Online
View Journal | View Issue

Cite this: J. Mater. Chem. C, 2018, 6, 6733

The electronic properties of $CH_3NH_3PbI_3$ perovskite surfaces tuned by inverted polarities of pyridine and ethylamine†

Tingting Shi, [ab] Qiang Teng,[c] Xiao-Bao Yang, [ac] Hin-Lap Yip *[ad] and Yu-Jun Zhao *[ac]

Received 25th January 2018,
Accepted 21st May 2018

DOI: 10.1039/c8tc00409a

rsc.li/materials-c

Lead (Pb)-based halide perovskites with enhanced solar cell performance and a larger open-circuit voltage were experimentally observed after the treatment of crystal surfaces with pyridine and amine-functionalized molecules. We model the Pb–I_2 terminated perovskite surfaces using density-functional theory and find that two small organic molecules, pyridine and ethylamine, interact with the surfaces and tune their electronic band gaps. When dopants on surfaces have parallel or antiparallel polarities with the orientation of methylammonium (MA = CH_3NH_3) molecules in bulk, the electronic properties of the perovskite surfaces will be remarkably different. We demonstrate that ethylamine and pyridine with antiparallel polarities can enlarge the band gaps of perovskite surfaces. The change of electronic properties is ascribed to the cancellation of the dipole moments caused by the pyridine/ethylamine and methylammonium molecules on surfaces. We further vary the polarities of MA molecules by interchanging the C and N atoms in a symmetric fashion for showing the influence of polarization on total energies, electronic properties and charge distributions.

Introduction

Due to the extraordinary optoelectronic properties: the appropriate and tunable band gap values, outstanding charge carrier mobility, long diffusion length and high absorption coefficient,[1–3] the power conversion efficiency of methylammonium (MA) lead-based tri-halide perovskite solar cells has made an impressive leap from less than 5% to over 22% within eight years.[4–14] Moreover, the possibility of fabricating the perovskite solar cells based on low cost solution processes makes them an even more appealing photovoltaic technology. Typically, solution-processed thin films generally contain a large amount of defect states such as surface trap states, which may act as recombination centers in the device. However, theoretical calculations suggested that the perovskite films appear against this trend, as the impurity levels caused by the defect states tend to locate outside the band gap, making them insensitive to trap-induced recombination loss.[15–17] Indeed, experimentally it was shown that the presence of surface traps in perovskite films could be one of the major factors that promote charge recombination and limits the performance of the solar cell devices.[18,19] To circumvent this problem in perovskite cells, surface passivation using Lewis bases including thiophene and pyridine was applied.[20,21] Recently, it was also reported that electron-rich functional groups such as amines[22] and fullerenes[23] can also passivate the surface traps of perovskite films. A similar strategy has also been adopted to improve the perovskite light emitting devices by tuning the interfacial properties and microstructures of the perovskite films, showing the importance of interface control in perovskite optoelectronic devices.[24–26]

Recently scanning tunneling microscopy studies have revealed that the structural characteristics of perovskite surfaces were sensitive to the polarizations caused by MA molecules.[27] Density functional theory (DFT) calculations elucidated that the electronic structures of perovskite surfaces were highly dependent on the orientations of MA organic cations.[15,28] Therefore, designing suitable interfacial structures that are favorable for charge extraction from the perovskite semiconductors is extremely important for making efficient solar cells and there is a requirement for a better understanding of the effect of molecular surface passivation and the orientation of MA organic

[a] School of Materials Science and Engineering, South China University of Technology, Guangzhou, Guangdong 510640, China. E-mail: msangusyip@scut.edu.cn, zhaoyj@scut.edu.cn
[b] Siyuan Laboratory, Guangzhou Key Laboratory of Vacuum Coating Technologies and New Energy Materials, Department of Physics, Jinan University, Guangzhou 510632, China
[c] Department of Physics, South China University of Technology, Guangzhou, Guangdong 510640, China
[d] State Key Laboratory of Luminescent Materials and Devices, South China University of Technology, Guangzhou, Guangdong, 510640, China

† Electronic supplementary information (ESI) available. See DOI: 10.1039/c8tc00409a

cations on the interfacial electronic properties of perovskites. What makes even more complicated is that the surface passivation molecules typically possess dipole moments, which could further interact with the intrinsic polarization triggered by the orientation of MA molecules, and collectively influence the structural and electronic properties of perovskite surfaces. The ferroelectric domains in the solution-processed $CH_3NH_3PbI_3$ perovskite thin films were observed directly and the researchers have found that reversible switching of the domains could be realized by poling with DC biases.[29] Moreover, the related first-principles calculations based on 3D periodic boundary conditions also revealed that the ferroelectric structure with polarization is globally stable.[30] Although there was discrepancy between the theoretical and experimental results, several experimental pathways were mentioned to obtain the apparent ferroelectric behavior. Consequently, the polarization induced by the ferroelectric effect can influence the charge separation and the carrier lifetime. Also, the ferroelectric effect probably affects the open circuit voltages of perovskite cells.[29] However, the distinctive interaction and the intrinsic mechanism between perovskite surfaces and other small molecules with polarities are still underexplored.

In this paper, we have investigated the structural and electronic properties of perovskite surfaces doped with two different molecules, ethylamine and pyridine, which are known to be efficient surface passivation elements for perovskite solar cells, exemplified with the cubic phase. After considering the strong structural correlations between perovskite surfaces and pyridine/ethylamine, we speculate that the interaction mechanism of polarization originates from the organic molecules, which can tune the electronic band gaps of the whole system. The pyridine atom-doped system with the anti-parallel finally enlarged band gap is highly consistent with the experimental results.[20] The ethylamine atom induced similar influence to the perovskite surface and further broadened the band gap due to its stronger absorption energy.

Theoretical methods

The surface calculations are based on a slab supercell with four $Pb–I_6$ octahedral layers and a 15 Å vacuum region next to the slabs. The supercell of the pure surface contains 102 or 204 atoms. The DFT calculations were performed using the Vienna *ab initio* simulation package (VASP) code[31] with the standard frozen-core projector augmented-wave (PAW) method.[32,33] The generalized gradient approximation (GGA) of the Perdew–Burke–Ernzerhof (PBE)[34] functional was employed for the exchange–correlation potential. The cut-off energy for basis functions was 400 eV and the *k*-point mesh was obtained using the Monkhorst–Pack[35] method with a grid density of $4 \times 4 \times 1$ for the slab. Atoms were relaxed until the Hellmann–Feynman forces on them were below 0.05 eV $Å^{-1}$. The band gap errors in using GGA and the neglect of spin-orbit coupling (SOC) are cancelled with each other in occurrence, as the effect of SOC on $MAPbI_3$ due to strong relativistic effects of Pb has been discussed in the literature.[36–40] Therefore, the GGA calculations are accepted to predict the experimental band gap without any underestimation. We also calculated the surfaces using a van der Waals density functional (vdw-DF) proposed for molecules, and the correction based on the DFT-D2 method of Grimme was used.[41]

Adsorption energy was considered in the surface energy calculations. The final adsorption energy of molecules was determined from the total energy of the doped system with any small molecules E_{tot}, the total energy of the pure surface before doping E_{surf} and the individual total energy of this molecule E_{mol}, as shown below:

$$E_{ad} = E_{tot} - (E_{surf} + E_{mol})$$

Results and discussion

In this paper, we consider the cubic (001) Pb–I terminated perovskite surfaces, which exhibit similar characteristics to the tetragonal (110) Pb–I terminated surfaces. Pb–I terminations are the most common one, which are often discussed for understanding the characteristics of the perovskite surface. It is much easier to treat the adsorption of pyridine and ethylamine on surfaces of the cubic phase, though it is typically available at high temperature. In fact, we have conducted calculations of the tetragonal Pb–I terminated perovskite surfaces, where similar polarization exists although slightly weaker than that of the cubic phase. In addition, we examine the surface energies with different layers and finally choose the one with converged energy, which has four $Pb–I_6$ octahedral cells and four MA molecules layers, as shown in Fig. 1.

In our calculation, we study the interaction between the perovskite surface and different small molecules, exemplified with pyridine (C_5H_5N) and ethylamine (C_2H_7N). Both pyridine and ethylamine molecules have polarities. When we dope them onto the top and bottom surfaces, they will influence the polarity differently due to the existing MA polarities on the perovskite surface. As shown in Fig. 1, we can see that the dopants pyridine and ethylamine have an inverted polarity along the *z* direction, compared with the MA polarity (along the C–N direction) of the perovskite surface.[42] In previous experimental observation, Snaith's group found that pyridine passivated the surface after the Lewis treatment and the doped system has a larger open-circuit voltage.[21] We then calculate the total density of states (TDOS) of the pure system and the doped ones. Fig. 2 shows that the band gap of the doped system is larger than that of the pure system. We further compare the orbital characteristics around the Fermi level in Fig. 2(b) and predicted that possible transitions occurred after the passivation of pyridine and ethylamine. Comparison of the calculated DOS indicates a possible wider photon transition after the doping of amines which has already been confirmed by a blue shift in the photoluminescence (PL) spectrum experimentally.[22]

Furthermore, the band structures of these three systems are calculated, as shown in Fig. 3. We obtain that the band gap of the pure system is 1.07 eV, while those of pyridine and ethylamine-doped surfaces are 1.26 eV and 1.31 eV, respectively. These correspond to a remarkable increase of band gaps of 0.19 eV and 0.24 eV due to pyridine and ethylamine doping.

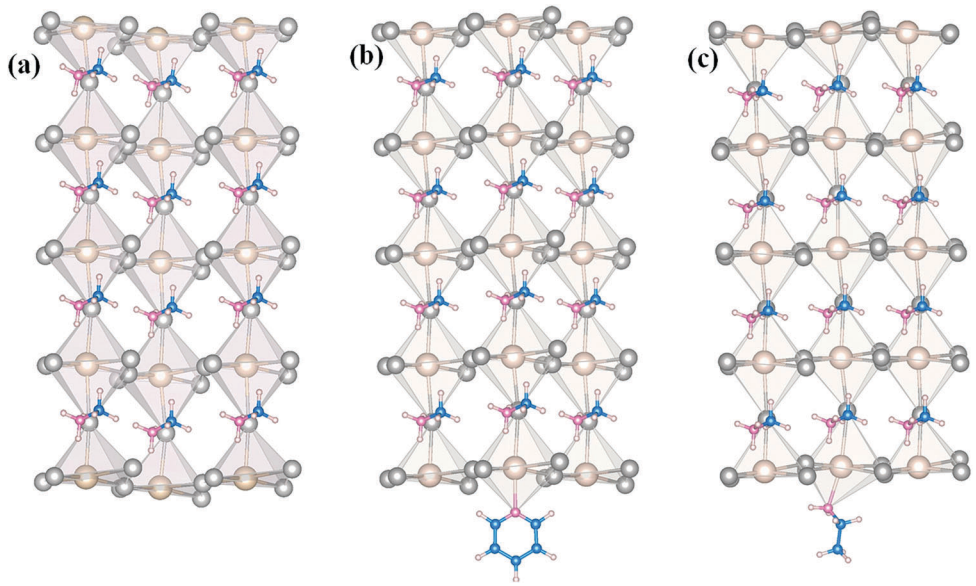

Fig. 1 Atomic models of the (a) pure (001) Pb–I terminated surface (b) doped surface with pyridine, and (c) doped surface with ethylamine. I, Pb, C, N, and H atoms are represented as grey, light orange, blue, pink, and small light pink balls, respectively.

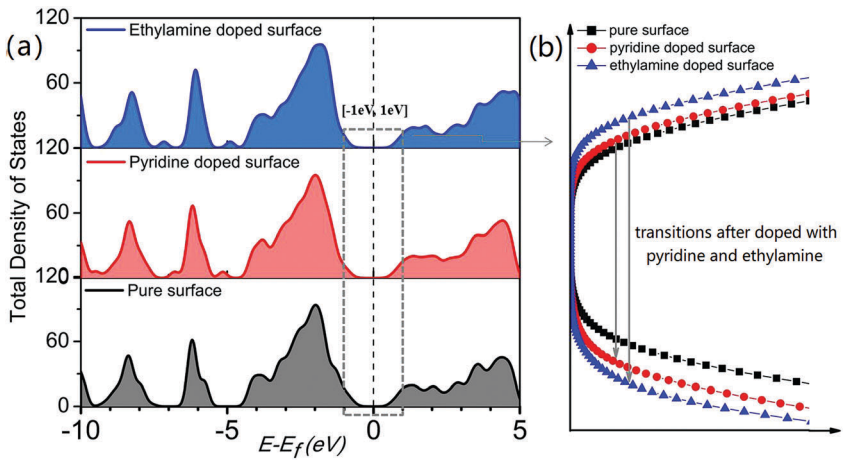

Fig. 2 (a) TDOS of the pure perovskite surface and doped systems with pyridine, ethylamine, and (b) the comparison of DOS around VBM and CBM among the pure surface, the surface doped with pyridine and the surface doped with ethylamine. The black line shows the pure system, while the red and blue ones correspond to the pyridine and ethylamine doped systems, respectively.

The change in the band gaps affected by organic atoms will vary correspondingly according to the different adsorption energies. The adsorption energy of ethylamine on the perovskite surface is −0.76 eV, smaller than that of pyridine. Therefore, the change in the band gaps of the ethylamine-doped surface is larger.

In addition, we find that the changes of band gaps were less than 5% when the van der Waals interaction is considered, without affecting the trend in band gaps due to molecular adsorption. Furthermore, considering the coverage concentration of the dopant, we investigate the pyridine-doped perovskite surface with double size, including 1 pyridine molecule and 204 perovskite atoms. We also find that the band gap of this system still increases after the doping of pyridine, but the value is 1.20 eV, smaller than that of the previous pyridine-doped system.

We further investigate the structural and electronic properties of the molecule-doped perovskite systems to understand more on the increase of band gaps. On the one hand, the perovskite surfaces are sensitive to the change in Pb–I bond lengths because of the structural distortion. In the ESI,† we compare the band gaps of the relaxed doped system with and without a dopant, and testify the direct influence due to the structural distortion. In Fig. S1 (ESI†), the energy gap become 0.78 eV from 1.26 eV after pyridine was removed in the inverted direction, compared with the value of 1.30 eV from 1.10 eV when pyridine was removed in the parallel direction. So after removing the dopants, the obvious changes in band gaps show

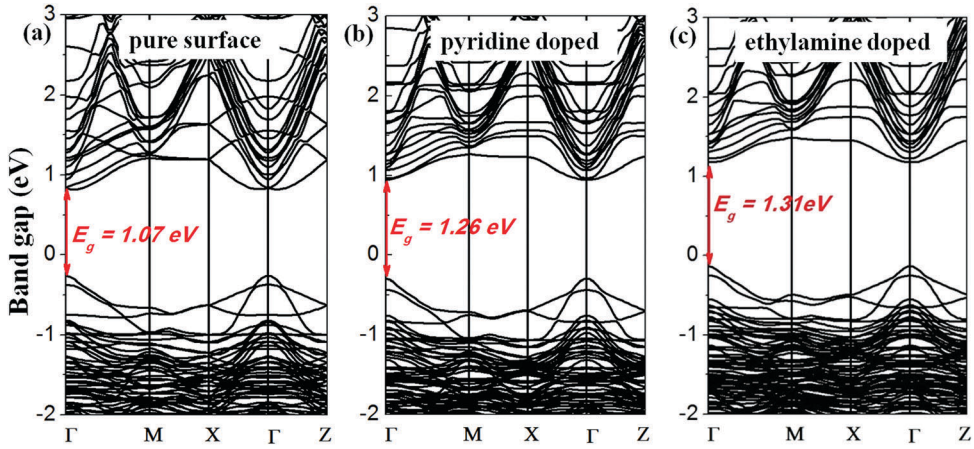

Fig. 3 Band structures of the (a) pure perovskite surface, (b) perovskite surface doped with pyridine and (c) perovskite surface doped with ethylamine.

two opposite trends due to the structural distortions caused by previous dopants.

On the other hand, we emphasize the influence of MA and find that the polarity of the whole system tunes the electronic properties of perovskite surfaces. The surface MA cations tilted at an angle with respect to the horizontal direction, resulting in the net polarization along the *z*-axis, which not only affects the structural characteristics, but also changes the electronic properties of perovskite surfaces. Here, we calculate the surface slabs with 8MA molecules to explore the influence caused by the change of MA polarity. We tune the polarity by interchanging the C and N position of the individual MA molecule, and then obtain the opposite polarity in comparison to the previous one. Suppose one MA is the unit of polarization here, we can vary the MA polarization by tuning the C–N polarities from 0MA, 2MA, 4MA, 6MA to 8MA, as shown in the insets in Fig. 4. Here 8MA and 0MA correspond to the maximum and minimum polarization scenarios, respectively. In our calculation, the whole system with the ferroelectric domain 8MA is the most stable one. Previous research also affirmed that there are local domains with consistently orientated MA molecules in the perovskite systems.[43–46] Furthermore, we calculated the corresponding total energy of the systems and their corresponding band gap values. We found that the band gap value decreases as the polarization increased. The largest band gap value of the perovskite surface with 0MA polarity is 1.6 eV, while the smallest value of the surface slab with 8MA polarity is 1.07 eV. The band gap shrinks as the polarization along the *z*-axis increases due to the electrical field triggered by the intrinsic dipole moments. Considering the decrease of total energies, we ascribed this trend to the Coulomb repulsion of MA molecules in the parallel layer. Therefore the surface system with 0MA, whose polarity is indicated by orange arrows in Fig. 2, is energy unfavorable, due to the repulsion between C–C and N–N of the nearby molecules. The surface with 8MA polarity, which has the consistent atomic sequence along the *z*-axis, is the most stable one.

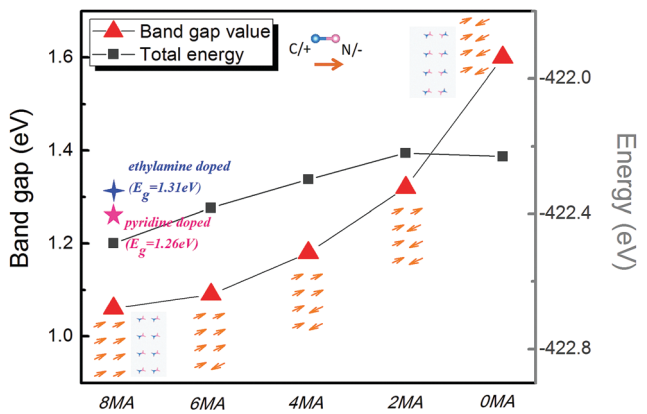

Fig. 4 Total energy and band gap influenced by MA polarities and the corresponding changes caused by pyridine and ethylamine.

In order to summarize the interaction mechanism between the perovskite surface and the dopants, and the polarization effect on the electronic properties of the perovskite surface, we draw the schematic diagram, in Fig. 5, which shows the band gap change under an intrinsic electric field along C–N directions. The electron charges like to gather into the top sites of the valence band level after the electric field makes all band levels tilted and the band gap decreases under the influence of intrinsic dipoles.[47] Obviously, the charge of the valence band maximum (VBM) should be prone to distribute on the top surface when the surface has the highest MA polarization, shown in Fig. 5(a). While the polarization of the system is canceled, the VBM charge will be distributed uniformly on both two outermost perovskite surfaces, in line with that shown in Fig. 5(c). As a result, we conclude that the polarization caused by the molecules significantly affects the total energy, the electronic properties and the charge distribution of the perovskite surfaces.

The role of polarization in the halide perovskite system can be further demonstrated by the doping of the pyridine/ethylamine molecule. We here design two scenarios of doping of these molecules on the perovskite surfaces: doping the pyridine/ethylamine molecule on the top and on the bottom outermost perovskite surface, respectively. It is clear that when the molecule is

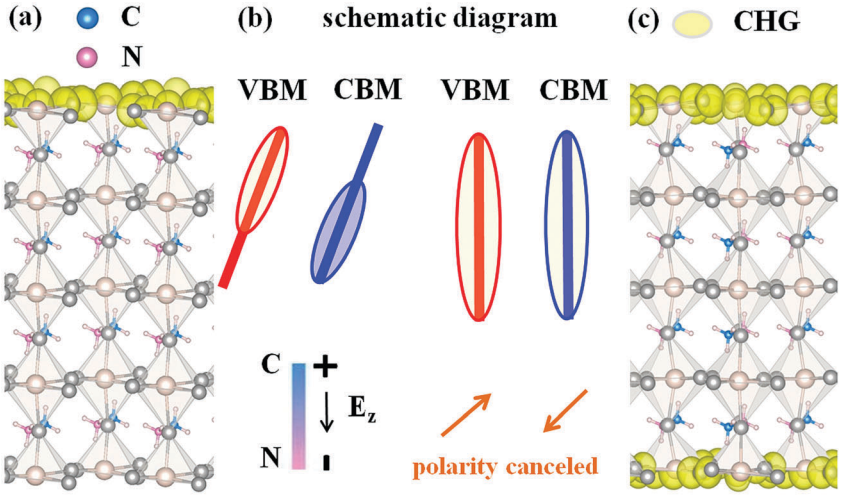

Fig. 5 The VBM charge distribution of the perovskite surface with 8MA (a) and 0MA (b) polarities, along with the schematic diagram of the VBM and CBM charge distribution with and without an electric field induced by dipole moments.

Table 1 The band gap values of the doped systems and their corresponding adsorption energy

Impurity	Doped direction	Band gap value (eV)	Adsorption energy (eV)
Pyridine	Consistent polarity	1.10	−0.67
	Inverted polarity	1.26	−0.72
Ethylamine	Consistent polarity	1.32	−0.81
	Inverted polarity	1.31	−0.76

placed on the top/bottom surface, the polarity of the molecule is parallel/antiparallel to the *z*-projection of the intrinsic polarization of the bulk MA molecules. Obviously, the band gap value of pyridine doped on the top surface is smaller than that of pyridine doped on the bottom surface according to our early argument. This is confirmed by our calculations, as listed in Table 1. For the ethylamine doped systems, both methods of doping will increase the band gaps largely. The dopants with different polarizations will affect the band gaps of perovskite surfaces differently. The band gaps of the doped systems will increase after previous polarizations were canceled by doping with anti-parallel polarity of pyridine/ethylamine on surfaces. Moreover, the value of the band gap of the ethylamine-doped surface is larger than that of the pyridine-doped surface because of its higher adsorption energy on the perovskite surface, which also means that the ethylamine has more structural influence on the electronic properties, but the pyridine molecule exhibits a larger polarization effect. In Table 1, we can observe the different adsorption energies of each dopant, different doping methods in our calculations and the band-gap changes in all the corresponding cases.

Conclusions

Organic molecules pyridine and ethylamine lead to the obvious change of the electronic properties of the doped perovskite surfaces. Through doping the polarized molecules onto the surfaces, the band gap values can be tuned. Herein, we conclude the trends in total energies and band gap values as we change the intrinsic symmetric fashion of MA molecules and find the mechanism caused by the varied polarization. We propose that two dopants and doped types, either with consistent polarity or inverted polarity, will tune the electronic properties of the perovskite surface differently. The decrease in the polarization of the perovskite surfaces caused by the inverted polarity of pyridine and ethylamine will lead to an increase in the band gap. The increase in the band gap after doping with pyridine/ethylamine, on the one hand, indicates a larger open-circuit voltage in the experiment, and on the other hand, helps the wider photon transition and the blue shift of the experimental photoluminescence spectrum become possible.

Conflicts of interest

There are no conflicts to declare.

Acknowledgements

This work was supported by NSFC (Grant 11574088, 51431001, 51573057, 91733302), the China Postdoctoral Science Foundation (Grant 2017M612646), the Foundation for Innovative Research Groups of the National Natural Science Foundation of China (Grant No. 51621001), and the Natural Science Foundation of Guangdong Province of China (Grant No. 2016A030312011). The Computer Times at the National Supercomputer Center in Guangzhou (NSCCGZ) is gratefully acknowledged. T. S. also acknowledges the discussion with Prof. Pengyi Liu, Prof. Feng Hong and Prof. Wanjian Yin.

References

1 G. Xing, N. Mathews, S. Sun, S. S. Lim, Y. M. Lam, M. Grätzel, S. Mhaisalkar and T. C. Sum, *Science*, 2014, **342**, 344.

2 W. J. Yin, T. Shi and Y. Yan, *Adv. Mater.*, 2014, **26**, 4653–4658.
3 S. D. Stranks, G. E. Eperon, G. Grancini, C. Menelaou, M. J. P. Alcocer, T. Leijtens, L. M. Herz, A. Petrozza and H. J. Snaith, *Science*, 2014, **342**, 341.
4 M. A. Green, K. Emery, Y. Hishikawa, W. Warta, E. D. Dunlop, D. H. Levi and A. W. Y. Ho-Baillie, *Prog. Photovoltaics*, 2017, **25**, 3–13.
5 https://www.nrel.gov/pv/assets/images/efficiency-chart.png.
6 J. H. Im, C. R. Lee, J. W. Lee, S. W. Park and N. G. Park, *Nanoscale*, 2011, **3**, 4088–4093.
7 M. M. Lee, J. Teuscher, T. Miyasaka, N. T. Murakami and H. J. Snaith, *Science*, 2011, **338**, 643.
8 H. S. Kim, C. R. Lee, J. H. Im, K. B. Lee, T. Moehl, A. Marchioro, S. J. Moon, R. Humphry-Baker, J. H. Yum, J. E. Moser, M. Gratzel and N. G. Park, *Sci. Rep.*, 2012, **2**, 591.
9 J. Burschka, N. Pellet, S. J. Moon, R. Humphry-Baker, P. Gao, M. K. Nazeeruddin and M. Gratzel, *Nature*, 2013, **499**, 316–319.
10 D. Liu and T. L. Kelly, *Nat. Photonics*, 2013, **8**, 133–138.
11 M. Liu, M. B. Johnston and H. J. Snaith, *Nature*, 2013, **501**, 395–398.
12 J. H. Noh, S. H. Im, J. H. Heo, T. N. Mandal and S. I. Seok, *Nano Lett.*, 2013, **13**, 1764–1769.
13 W. S. Yang, J. H. Noh, N. J. Jeon, Y. C. Kim, S. Ryu, J. Seo and S. Seok, *Science*, 2015, **348**, 1234–1237.
14 A. Guerrero, J. You, C. Aranda, Y. S. Kang, G. Garcia-Belmonte, H. Zhou, J. Bisquert and Y. Yang, *ACS Nano*, 2016, **10**, 218–224.
15 W. Meng, Z. Xiao, T. Shi, J. Wang and Y. Yan, Absence of Surface Trap States in Actual $CH_3NH_3PbI_3$ Perovskite-the Effects of Rapid Organic Cation Rotation, unpublished.
16 J. Haruyama, K. Sodeyama, L. Han and Y. Tateyama, *J. Phys. Chem. Lett.*, 2014, **5**, 2903–2909.
17 W. Geng, C.-J. Tong, Z.-K. Tang, C. Yam, Y.-N. Zhang, W.-M. Lau and L.-M. Liu, *J. Materiomics*, 2015, **1**, 213–220.
18 A. Abate, M. Saliba, D. J. Hollman, S. D. Stranks, K. Wojciechowski, R. Avolio, G. Grancini, A. Petrozza and H. J. Snaith, *Nano Lett.*, 2014, **14**, 3247–3254.
19 T. Leijtens, S. D. Stranks, G. E. Eperon, R. Lindblad, E. M. J. Johansson, I. J. McPherson, H. Rensmo, J. M. Ball, M. M. Lee and H. J. Snaith, *ACS Nano*, 2014, **8**, 7147–7155.
20 N. K. Noel, A. Abate, D. S. Stranks, S. E. Parrott, V. M. Burlakov, A. Goriely and H. J. Snaith, *ACS Nano*, 2015, **8**, 9815–9821.
21 D. W. deQuilettes, S. M. Vorpahl, S. D. Stranks, H. Nagaoka, G. E. Eperon, M. E. Ziffer, H. J. Snaith and D. S. Ginger, *Science*, 2015, **348**, 683–686.
22 C. Sun, Z. Wu, H.-L. Yip, H. Zhang, X.-F. Jiang, Q. Xue, Z. Hu, Z. Hu, Y. Shen, M. Wang, F. Huang and Y. Cao, *Adv. Energy Mater.*, 2016, **6**, 1501534.
23 Y. Xing, C. Sun, H. L. Yip, G. C. Bazan, F. Huang and Y. Cao, *Nano Energy*, 2016, **26**, 7–15.
24 Z. Chen, C. Zhang, X. F. Jiang, M. Liu, R. Xia, T. Shi, D. Chen, Q. Xue, Y. J. Zhao, S. Su, H. L. Yip and Y. Cao, *Adv. Mater.*, 2017, **29**, 1603157.
25 M. Yuan, L. N. Quan, R. Comin, G. Walters, R. Sabatini, O. Voznyy, S. Hoogland, Y. Zhao, E. M. Beauregard, P. Kanjanaboos, Z. Lu, D. H. Kim and E. H. Sargent, *Nat. Nanotechnol.*, 2016, **11**, 872–877.
26 J. Wang, N. Wang, Y. Jin, J. Si, Z. K. Tan, H. Du, L. Cheng, X. Dai, S. Bai, H. He, Z. Ye, M. L. Lai, R. H. Friend and W. Huang, *Adv. Mater.*, 2015, **27**, 2311–2316.
27 L. She, M. Liu and D. Zhong, *ACS Nano*, 2016, **10**, 1126–1131.
28 Q. Xu, A. Stroppa, J. Lv, X. Zhao, D. Yang, K. Biswas and L. Zhang, *Rotations of the organic molecules and their effects on optoelectronic properties in solar hybrid halide perovskites*, to be published.
29 Y. Kutes, L. Ye, Y. Zhou, S. Pang, B. D. Huey and N. P. Padture, *J. Phys. Chem. Lett.*, 2014, **5**, 3335–3339.
30 Z. Fan, J. Xiao, K. Sun, L. Chen, Y. Hu, J. Ouyang, K. P. Ong, K. Zeng and J. Wang, *J. Phys. Chem. Lett.*, 2015, **6**, 1155–1161.
31 G. Kresse and J. Hafner, *Phys. Rev. B: Condens. Matter Mater. Phys.*, 1993, **47**, 558–561.
32 P. E. Blöchl, *Phys. Rev. B: Condens. Matter Mater. Phys.*, 1994, **50**, 17953–17979.
33 G. Kresse and D. Joubert, *Phys. Rev. B: Condens. Matter Mater. Phys.*, 1999, **59**, 1758–1775.
34 J. P. Perdew, K. Burke and E. Matthias, *Phys. Rev. Lett.*, 1996, **77**, 3865–3868.
35 H. J. Monkhorst and J. D. Pack, *Phys. Rev. B: Condens. Matter Mater. Phys.*, 1976, **13**, 5188–5192.
36 J. Even, L. Pedesseau, M. A. Dupertuis, J. M. Jancu and C. Katan, *Phys. Rev. B: Condens. Matter Mater. Phys.*, 2012, **86**, 205301.
37 J. Even, L. Pedesseau, J.-M. Jancu and C. Katan, *J. Phys. Chem. Lett.*, 2013, **4**, 2999–3005.
38 E. Mosconi, A. Amat, M. K. Nazeeruddin, M. Grätzel and F. De Angelis, *J. Phys. Chem. C*, 2013, **117**, 13902–13913.
39 E. Menéndez-Proupin, P. Palacios, P. Wahnón and J. C. Conesa, *Phys. Rev. B: Condens. Matter Mater. Phys.*, 2014, **90**, 045207.
40 P. Umari, E. Mosconi and F. De Angelis, *Sci. Rep.*, 2014, **4**, 4467.
41 S. Grimme, *J. Comput. Chem.*, 2006, **27**, 1787–1799.
42 Note: we also calculated the tetragonal PbI_2 terminated surface, similarly, the increased band gap was also triggered by the pyridine with antiparallel polarity, but the changed value is smaller than the cubic one due to the larger atomic structure and weaker polarization. In fact, only in the low temperature phase, the rotations of the C–N axis are restricted and free rotation of dipolar $CH_3NH_3^+$ are ruled out from the experimental observation. However, the real complicated thermodynamic situations still need to be explored in future.
43 A. M. Leguy, J. M. Frost, A. P. McMahon, V. G. Sakai, W. Kochelmann, C. Law, X. Li, F. Foglia, A. Walsh, B. C. O'Regan, J. Nelson, J. T. Cabral and P. R. Barnes, *Nat. Commun.*, 2015, **6**, 7124.
44 J. M. Frost, K. T. Butler and A. Walsh, *APL Mater.*, 2014, **2**, 081506.
45 J. M. Frost, K. T. Butler, F. Brivio, C. H. Hendon, M. V. Schilfgaarde and A. Walsh, *Nano Lett.*, 2014, **14**, 2584–2590.
46 A. Stroppa, D. Di Sante, P. Barone, M. Bokdam, G. Kresse, C. Franchini, M. H. Whangbo and S. Picozzi, *Nat. Commun.*, 2014, **5**, 5900.
47 Y.-M. Tan, Y.-J. Zhao, L.-B. Luo, X.-B. Yang and H. Xu, *RSC Adv.*, 2014, **4**, 44004–44010.

